Selective generation of narrow-band harmonics by a relativistic laser pulse interaction with a detuned plasma grating

Shaoyi Wang,[1,2] Fang Tan,[1,2] Zuhua Yang,[1,2] Yuchi Wu,[1,2] Xiaohui Zhang,[1,2] Minghai Yu,[1,2] Yue Yang,[1,2] Yonghong Yan,[1,2] Bin Zhu,[1,2] Lai Wei,[1,2] Quanping Fan,[1,2] Jingqin Su,[1,2] Yuqiu Gu,[1,2] and Weimin Zhou[1,2,*]

[1]*Research Center of Laser Fusion, CAEP, P. O. Box 919 986, Mianyang 621900, China*

[2]*The Sciences and Technology on Plasma Physics Laboratory, CAEP, Mianyang 621900, China*

(Received 7 September 2021; accepted 15 May 2022; published 21 June 2022)

The spectral characteristics of high-order harmonics generated by the interaction of a linearly polarized relativistic laser pulse with a plasma grating target are investigated. Through particle-in-cell simulations and an analytical model, it is shown that a plasma grating target with periodic structure can select special harmonics with integer multiples of the grating frequency, and that low-order harmonics with frequencies being integer times of the laser frequency are generated nearly parallel to the target surface from a Fresnel zone plate target with an aperiodic structure. Spectral control of the harmonics can be achieved by introducing a correction factor β to the radius formula of the Fresnel zone plate, which can create a slightly detuned plasma grating, and then only the narrow-band harmonics can be selected nearly parallel to the target surface. The center order of the narrow-band harmonics can be tuned by adjusting the correction factor β, while the bandwidth of the harmonics can be selected by adjusting the other parameter λ_f of the detuned plasma grating.

DOI: 10.1103/PhysRevE.105.065207

I. INTRODUCTION

High harmonic generation (HHG) from a gas or solid medium is an extreme nonlinear process, which contains a very broad range of frequencies that are generally integer multiple of the fundamental laser frequency. HHG is mainly used to generate a table-top attosecond pulse [1–9], which is an important tool for studying the electronic dynamics in atoms and molecules [10–12]. Nowadays, attosecond science is based mainly on HHG in gas media [13–22], which allows the generation of isolated attosecond pulses on the nanojoule to few-microjoule energy level with photon energies up to sub-keV. Due to the ionization threshold of the gas, the conversion efficiency of the attosecond pulse is limited. Relativistic harmonics generated by interaction of intense laser fields with solid surfaces is a promising way for the production of intense attosecond radiation [23–34]. There are two main HHG mechanisms identified on flat solid plasma: coherent wake emission (CWE) [35] and relativistic oscillating mirror process (ROM) [4]. Many efforts have been made to generate an isolated attosecond pulse, and a number of techniques have been experimentally carried out, such as "attosecond lighthouse" [6,36], "non-collinear optical gating" [37], "few-cycle regime" [38], and so on.

Another purpose of the high harmonics is providing particular harmonic frequencies for some potential application [39–41]. Among the reported schemes, a particular group of high-order harmonics has been selected by using two-color counter-rotating circularly polarized laser fields owing to the symmetry of the laser fields and the related conservation laws [42]. Selected enhancement of high-order harmonics can be also achieved by modifying the plasma density ramp [43]. Another spectrum control scheme is adopting a diffraction grating with a periodic structure [44,45], strong coherent emission at the wavelength of the grating period and its harmonics is generated nearly parallel to the target surface, which is forecast by Lavocat-Dubuis *et al.* [44,45]. Their theoretical predictions have been confirmed experimentally by Cerchez *et al.* and Cantono *et al.* [46,47]. Even though much efforts have been made to select a group harmonics from a periodic structure target [48–51], the methods of controlling the harmonic spectrum to isolate particular harmonics with a narrow band remain limited.

As mentioned above, laser engineering and target engineering techniques are needed to achieve selective harmonic enhancement. For high-peak-power laser systems, laser engineering techniques are still a challenging task. The development of new target engineering techniques makes the precise control of plasma grating structures possible with a microscale and nanoscale [24,52,53]. In this paper, we propose another target engineering technique to achieve spectral control. The Fresnel zone plate with an aperiodic structure only selects low-order harmonics with frequencies being integer times of the laser frequency nearly parallel to the target surface due to the interference effect. By introducing a correction factor β to the radius formula of the Fresnel zone plate target, phase matching condition of enhancement at narrow-band orders can be satisfied, and then the near-surface narrow-band harmonics can appear. The center order of the narrow-band harmonics can be tuned by adjusting the correction factor β, while the bandwidth of the harmonics can be selected by adjusting the other parameter λ_f of the detuned plasma grating.

*zhouwm@caep.cn

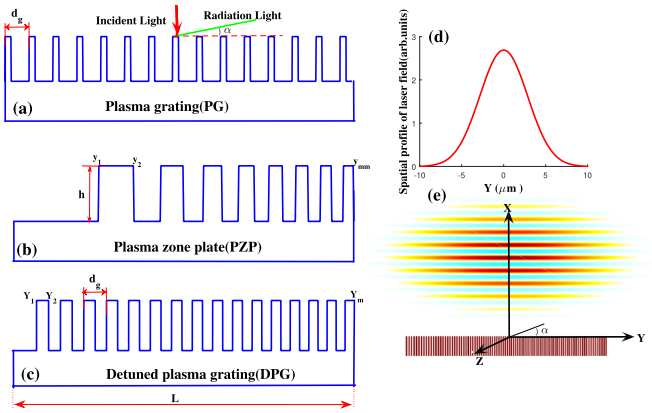

FIG. 1. Interaction geometry for a plasma grating target (a), plasma zone plate (b), or detuned plasma grating (c), h is the height of the zone; the spatial profile of laser field component shown in (d), and the electric field is polarized along $\hat{Y}$, the interaction configuration between an intense laser pulse and a detuned plasma grating is shown in (e).

II. MODE AND THEORETICAL ANALYSIS

The interaction configurations between the intense laser pulse and the plasma grating (PG), plasma zone plate (PZP), and detuned plasma grating (DPG) are shown in Fig. 1, and the corresponding target parameters are listed in Table I. The linearly polarized high intensity laser is normally incident on the target in $\hat{X}$ direction, and α is the emitting angle of the harmonics, which is shown in Fig. 1(e). For the plasma grating target, the grating period d_g can be designed as a quarter of the laser wavelength λ_0, and the depth h of the grating grooves is set as $\lambda_0/8$, and the width w_i is $\lambda_0/16$, the length L is set as 8 μm which is shown in Fig. 1(a). The configuration of the plasma Fresnel zone plate is shown in Fig. 1(b), the radial coordinate y_i can be expressed as $y_i = \sqrt{if_0\lambda_f}$, where i denotes the number of the zone, f_0 and λ_f are the focus and wavelength of the emitting light. Due to the diffraction effect, the zone plate can usually achieve to focus the light with a particular wavelength λ_f on $\hat{X}$ axis. Suppose each zone (i.e., the protuberance) is considered as a light point, the light points with the wavelength λ_f are focused to the coordinate $(0, \beta)$ along $\hat{X}$ axis by the above Fresnel zone plate, the optical path difference between the light points from the origin (0,0) and the coordinate $(y_i, 0)$ of $\hat{Y}$ axis is $\sqrt{(y_i)^2 + \beta^2} - \beta$. In order to generate harmonics parallel to $\hat{Y}$ axis, the same optical path difference should be achieved at $\alpha = 0^\circ$. The radius formula of the zone plate is modified by introducing a correction factor β, and the modified radial coordinate $(Y_i, 0)$ is expressed as $Y_i = \sqrt{if_0\lambda_f + \beta^2} - \beta$. The structure is similar to the grating, which is shown in Fig. 1(c). The width of each groove is variational and the height h is λ_0.

TABLE I. A table of the three target parameters.

Type	Length L	Period	Radial coordinate
PG	8 μm	$d_g = \lambda_0/4$	$y_{2i-1} = i\lambda_0/4,\ y_{2i} = y_{2i-1} + w_i$
PZP	8 μm	d_g is aperiodic	$y_i = \sqrt{if_0\lambda_f}$
DPG	8 μm	d_g is aperiodic	$Y_i = \sqrt{if_0\lambda_f + \beta^2} - \beta$

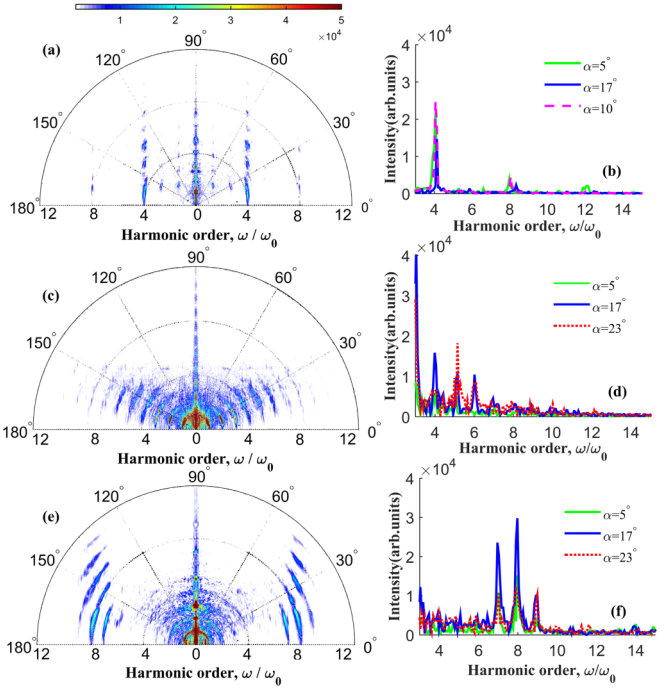

FIG. 2. The angular distribution of the radiation intensity with harmonic order from the plasma grating target with the period $d_g = \lambda_0/4$ (a), (b), the plasma zone plate (c), (d), and detuned plasma grating (e), (f) simulated by PIC, the laser duration τ is set as 20 fs, f_0 is 20 μm, $\lambda_f = 100$ nm, $\beta = 15$ μm, and $L = 8$ μm.

The radiation spectra obtained from the above three different targets are studied with the two-dimensional particle-in-cell simulation code EPOCH [54]. A linearly polarized laser pulse with the wavelength $\lambda_0 = 800$ nm is normally incident. A Gaussian temporal profile of the laser normalized electric field amplitude $a_y = a_0 \exp[-\sqrt{2\ln 2}(t-\sigma)^2/\tau^2]$ with full-width-at-half-maximum (FWHM) duration $\tau = 20$ fs and $\sigma = 40$ fs is chosen, and the normalized laser amplitude $a_0 = 2.2$ corresponds to laser intensity of $I_0 \sim 1 \times 10^{19}$ W/cm^2. The laser pulse has a Gaussian transverse profile with a focal spot of 8 μm. The three targets have electron density $n_e = 20n_c$. The simulation box is composed of $25\lambda_0 \times 30\lambda_0$. Due to the limitation of computational resources, we reduce the spatial resolution as $\lambda_0/500 \times \lambda_0/500$ and the number of particles per cell as 36 only, and the background ion is carbon.

The angular distributions of the radiation intensity with harmonic order from the periodic and aperiodic structure targets simulated by PIC are shown in Fig. 2, the corresponding radiation spectra at the special angles are also present. The strong harmonic radiation from the interaction between the laser pulse and the grating target with the period $d_g = \lambda_0/4$ is generated nearly parallel to the target surface, and the harmonic frequency is an integer multiple of the grating frequency, which is shown in Figs. 2(a) and 2(b). The radiation spectrum at the emitting angle $\alpha = 5^\circ$, 17°, and 23° from the zone plate with aperiodic structure is shown in Figs. 2(c) and 2(d), low-order harmonics can be generated, and the intensity changes rapidly from strong to weak as the radiation frequency is increased. By adopting the detuned plasma grating shown in Figs. 1(c), 2(e), and 2(f), a narrow-band spectrum

from about 7th to 9th appears nearly parallel to the target surface, and the other harmonics are strongly suppressed, which means that, because of the interference enhancement of particular harmonics due to the modified aperiodic structure, the maximum intensity is emitted at the angle $\alpha = 17^\circ$.

In order to better understand the emitting characteristic of the interaction between the high intensity laser and the above plasma targets, an analytical model developed by Zhang *et al.* is adopted [51]. The radiated power per unit of solid angle of the nth (i.e., $n = \omega/\omega_0$) harmonic can be expressed as

$$\frac{dP_n}{d\Omega_0} = \left(\frac{\gamma m_e \omega_0 c}{2\pi e}\right)^2 F_n(n,\theta) K_n(\alpha), \tag{1}$$

where $\gamma = (1-\rho^2)^{-1/2}$, $\rho = v/c$, v is the electron quiver velocity in the laser field, c is the speed of light, m_e is the electric mass, and ω_0 and α are the laser frequency and the observation angle with respect to $\hat{Y}$. The radiation $K_n(\alpha)$ from a single electron oscillating in the linearly polarized field is

$$K_n(\alpha) = \frac{n^2 e^2 \omega_0^2}{2\pi c} \tan(\alpha)^2 J_n^2[n\rho\ \cos(\alpha)], \tag{2}$$

and the factor of the interference can be expressed as

$$F_n(n,\alpha) = \left|\sum_{y_i}^{L} \exp[-inx_i k_0 \cos(\alpha)]\right|^2, \tag{3}$$

where $x_i \cos(\alpha)$ is the light phase difference between the emitting rays from the origin (0,0) and the coordinate $(y_i, 0)$ of $\hat{Y}$ axis, and the wave vector of the laser is k_0. The term $F(\omega,\alpha)$ corresponds to the contribution of all the protuberances on the last harmonic radiation source. According to the previous works, the relativistic electron bunches can be generated by the interaction of a linearly polarized relativistic intensity laser field with the protuberance of the grating (or the zone plate). For convenience, when the focal spot of the laser is not less than the length of the plasma grating, the effect of the radiation K_ω on the spectral characteristics of harmonics can be neglected, and then the final harmonics are mainly effected by the term $F(\omega,\alpha)$. In the calculation, the radiation from each protuberance of the three targets is considered as a light line.

To clearly distinguish the physical process of the harmonic generated from the three different targets studied by PIC code, the results simulated by the analytical model are shown in Fig. 3, and the parameters are consistent as those in Fig. 2. Figure 3(a) shows the dependence of the interference factor F on the harmonic order ω/ω_0 and the emitting angle α for the plasma grating with the period $d_g = \lambda_0/4$. When the harmonic frequencies are integer multiples of the grating frequency, the match condition of harmonic enhancement is satisfied; interference factor F values observably show up near the surface directions, and then the harmonics with the order 4th (8th, 12th, and so on) are generated, which is shown in Figs. 2(a) and 2(b). Due to the aperiodic structure of the Fresnel zone plate, the interference factor F at the low order is strong, and as the harmonic order increases the value of F decreases rapidly, which is shown in Figs. 3(c) and 3(d). The results are consistent with those in Figs. 2(c) and 2(d). The correction factor β is introduced to modify the structure of the Fresnel zone plate, and is set to 15 μm, the interference

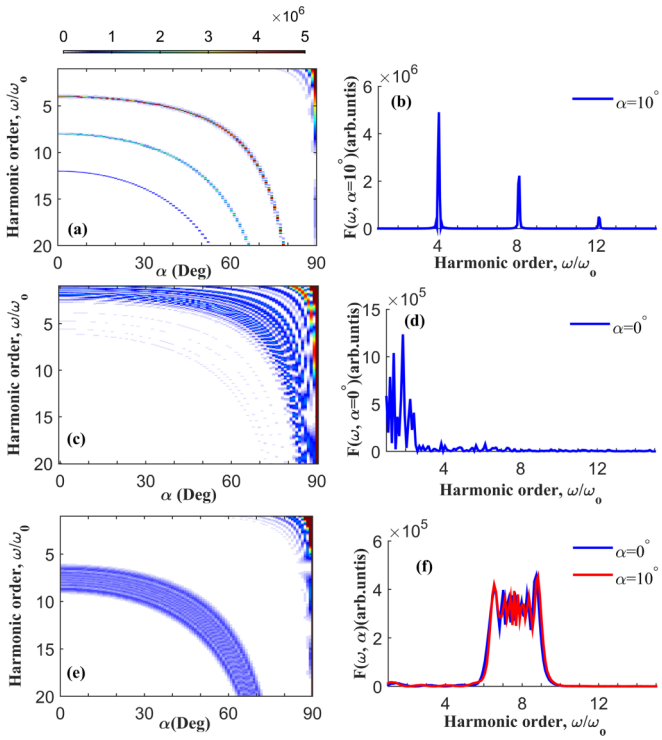

FIG. 3. The dependence of the interference factor F on the harmonic order ω/ω_0 and the emitting angle α calculated by the analytical model: (a) for the plasma grating, (c) for the zone plate, (e) for the detuned plasma grating; the corresponding radiation spectra at the different emitting angles are shown in (b), (d), and (f), and the parameters are consistent with those in Fig. 2.

factor F at the order ω/ω_0 from about 7th to 9th is much more intense than those of other harmonics at $\alpha = 0^\circ$ and 10°. Compared with Figs. 3(c) and 3(d), Figs. 3(e) and 3(f) present that only narrow-band harmonics are phase matched nearly parallel to the target surface when the target is the detuned plasma grating. The results calculated by the analytical model in Fig. 3 are consistent with the results in Fig. 2 simulated by PIC.

III. RESULTS AND DISCUSSION

The above results simulated by PIC and from analytic model show that the match condition of the enhanced emission from the periodic-structure grating target can be satisfied when the coherent emission is at the wavelength of the grating period and its harmonics, which is shown in Figs. 2(a), 2(b), 3(a) and 3(b). For the detuned plasma grating, an intuitive interpretation about the actual mechanics of the system could be given by the analysis of the aperiodic structure. The radial coordinate $(Y_i, 0)$ of the detuned plasma grating is expressed as $\sqrt{if_0\lambda_f + \beta^2} - \beta$, which is also written as $\beta(\sqrt{if_0\lambda_f/\beta^2 + 1} - 1)$. The wavelength d_g of the detuned plasma grating is expressed as

$$d_g(i) = \beta(\sqrt{(i+2)f_0\lambda_f/\beta^2 + 1} - \sqrt{if_0\lambda_f/\beta^2 + 1}). \tag{4}$$

From this formula, the detuned grating wavelength d_g is variable as i is increased. The term $f_0\lambda_f/\beta^2$ is small when i is 1, and we can Taylor expand the above formula (4) to get the

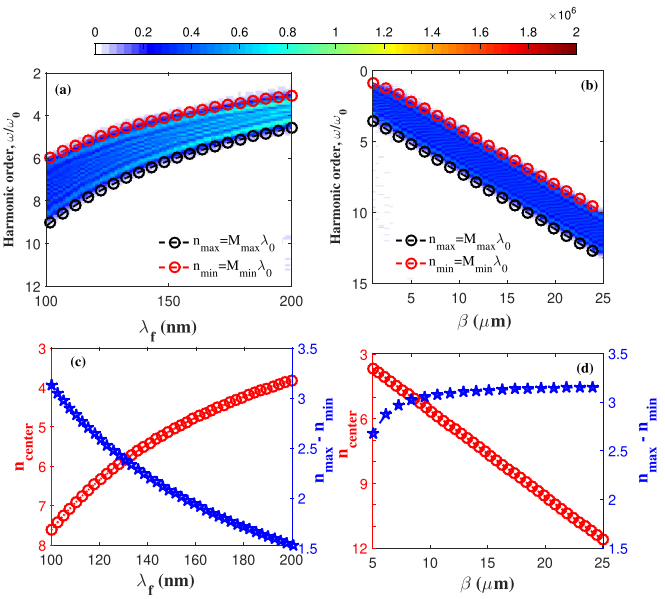

FIG. 4. The dependence of the interference factor F on (a) the parameter λ_f and (b) the correction factor β for the detuned plasma grating. The corresponding $n_{\max} - n_{\min}$ marked by blue stars and n_{center} marked by red circles are shown in (c) and (d), the other parameters are (a) $\beta = 15$ μm and (b) $\lambda_f = 100$ nm.

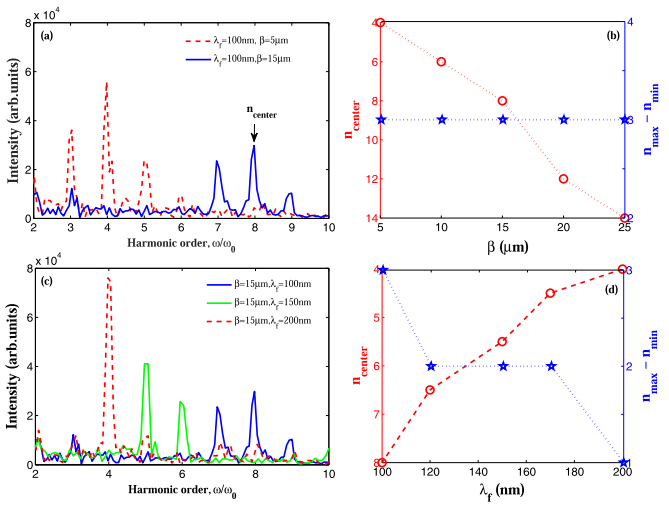

FIG. 5. The harmonic spectra at the emitting angle $\alpha = 17^\circ$ from the detuned plasma grating with different parameters β [(a) and (b)] and λ_f [(c) and (d)] simulated by PIC. The corresponding $n_{\max} - n_{\min}$ marked by blue stars and n_{center} marked by red circles are shown in (b) and (d), the other parameters are (a) $\lambda_f = 100$ nm and (b) $\beta = 15$ μm.

simple expression of d_g, which is expressed as

$$d_g(1) \simeq f_0\lambda_f/\beta. \tag{5}$$

From formula (5) above, it is shown that the wavelength of the detuned plasma grating is dependent on the parameters λ_f and β. As i gets large, the Taylor approximation is no longer valid, and $d_g(m)$ is minimal. The wave number of the detuned grating is defined as $M = 1/d_g$, the value of $M_{\min}$ is minimal when $i = 1$ and the value of $M_{\max}$ is maximal when $i = m$. The bandwidth of the enhanced harmonics from the detuned grating is determined by the number of grating wavelengths, and the minimal and maximal harmonic orders are considered as

$$n_{\min} \simeq M_{\min}\lambda_0, \;\; n_{\max} \simeq M_{\max}\lambda_0. \tag{6}$$

In Figs. 2 and 3, the parameter β is set as 15 μm, $f_0 =$ 20 μm, $\lambda_f = 100$ nm, and $L = 8\lambda_0$, and the minimal and maximal values of M are 7.57 μm^{-1} and 12.48 μm^{-1}, respectively. The corresponding harmonic orders are $n_{\min} = 6.05$ and $n_{\max} = 9.98$, and then the match condition of the harmonics from $n_{\min}$ to $n_{\max}$ can be satisfied, and then harmonics at the order 7th, 8th, and 9th can be selected. The above analysis results show that the narrow-band harmonics can be generated from the detuned plasma grating, which are consistent with the results calculated by the analytic model in Fig. 3(f).

The dependence of the interference factor F on the parameter λ_f and the correction factor β is studied by the analytical model in Fig. 4, and the results calculated by formula (6) are also shown. In Fig. 4(a), the correction factor β is considered as a constant, i.e., $\beta = 15$ μm, the emitting angle α is set 0°, and the other parameters are the same as those in Fig. 3(e). From Fig. 4(a), it is found that the frequencies of the harmonics which are phase matched are increased nonlinearly as λ_f is decreased. The minimal order $n_{\min}$ and maximal order $n_{\max}$ are calculated by formula (6), and the curves are in agreement with the result of the analytical model. The corresponding bandwidth $n_{\max} - n_{\min}$ and center frequency $n_{\text{center}} = (n_{\max} + n_{\min})/2$ of harmonics are shown in Fig. 4(c): $n_{\max} - n_{\min}$ is 3.13 and the n_{center} is 7.62 when λ_f is 100 nm, $n_{\max} - n_{\min}$ is 1.53 and the n_{center} is 3.82 when λ_f is 200 nm. In Fig. 4(b), the correction factor β is considered as a variable, the parameter λ_f is set to 100 nm, and the emitting angle α is also set to 0°; the other parameters are same as those in Fig. 3(e). It is shown that the frequencies of the harmonics which are phase matched are increased linearly as β is increased. The corresponding bandwidth $n_{\max} - n_{\min}$ and center frequency n_{center} are shown in Fig. 4(d): $n_{\max} - n_{\min}$ is 2.68 and the n_{center} is 3.67 when β is 5 μm, $n_{\max} - n_{\min}$ is 3.16 and the n_{center} is 11.61 when β is 25 μm, which shows that the bandwidth of the harmonics is varied slowly as the correction factor is increased.

The above results calculated by the analytical model and formula (6) show that the spectral characteristics of the narrow-band harmonics can be effected by the parameters λ_f and β. Figure 5(a) shows the harmonic spectra from the detuned plasma grating simulated by PIC when the correction factor β is adjusted, the parameter λ_f is set to 100 nm, and the β is variational; the other parameters are the same as those in Fig. 4(b). From Fig. 5(a), when β is 15 μm, the harmonics with orders 7th–9th are phase matched, while the harmonics with orders 3th–5th are phase matched as β is adjusted to 5 μm. The results in Figs. 5(a) and 5(b) show that the center frequency n_{center} can be tuned by increasing the correction factor β. The dependency of bandwidth $n_{\max} - n_{\min}$ on β is also shown in Fig. 5(b) marked by green stars, and $n_{\max} - n_{\min}$ is almost invariable as the β is increased, which is consistent with the result in Fig. 4(d). The effect of the parameter λ_f on the spectral characteristics of the narrow-band harmonics is

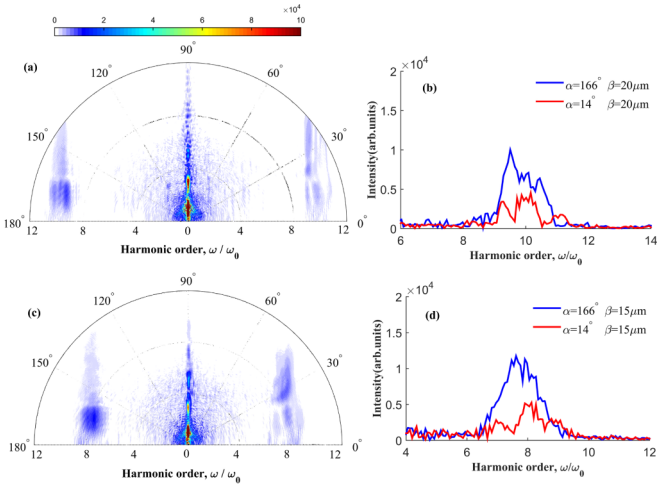

FIG. 6. The angular distribution of the harmonics driven by a few-cycle laser pulse from the detuned plasma grating with two correction factors β. (a), (b) $\lambda_f = 100$ nm, $\beta = 20$ μm, $\tau = 3$ fs; (c), (d) $\lambda_f = 100$ nm, $\beta = 15$ μm, $\tau = 3$ fs.

shown in Figs. 5(c) and 5(d), the parameter β is set to 15 μm, and the λ_f is variational; the PIC simulation results show that bandwidth $n_{\max} - n_{\min}$ is nonlinearly increased as the λ_f is decreased, $n_{\max} - n_{\min}$ is 3 as λ_f is 100 nm, and $n_{\max} - n_{\min}$ is 1 as λ_f is 200 nm, which is consistent with the results in Figs. 4(a) and 4(c).

In addition, the spectral characteristics of the harmonics driven by a few-cycle laser pulse from the detuned plasma grating are present in Fig. 6, the parameter λ_f is set to 100 nm, and the laser duration τ is 3 fs. Unlike the discrete harmonics driven by the multicycle laser pulse, a continuum harmonics can appear nearly parallel to the target surface. As shown in Figs. 6(a) and 6(b), when the correction factor β is set to 20 μm, the center frequency n_{center} of the harmonics at the emitting angle $\alpha = 166^\circ$ is about 9.58th, and the bandwidth $n_{\max} - n_{\min}$ is about 2.77. At the emitting angle $\alpha = 14^\circ$, the intensity of continuum harmonics is lower, and the spatial asymmetry of harmonics is due to the carrier-envelope phase of the few-cycle laser pulse. Figures 6(c) and 6(d) show that the continuum narrow-band harmonics from about 6.38th to 9.14th appeared at the emitting angle $\alpha = 166^\circ$, the correction factor β is set to 20 μm, the result shows that the corresponding center frequency n_{center} is 7.76th, and the bandwidth $n_{\max} - n_{\min}$ is about 2.76. The above results simulated by PIC are consistent with the results in Fig. 4.

The conversion efficiency of the harmonics driven by a multicycle laser pulse is affected by the laser spot size and plasma gradient scale length, which is shown in Fig. 7. The parameter λ_f is set to 100 nm, β is set to 15 μm, and the laser duration τ is 20 fs. As the laser spot size is increased, the harmonic efficiency is also enhanced, which is shown in Figs. 7(a) and 7(c). The 7th harmonic efficiency increases very fast while the efficiency of the 8th harmonic is gradually saturated. Figures 7(b) and 7(d) show the dependence of conversion efficiency of the harmonics on plasma gradient scale length L_p, and the laser spot size is set to 8 μm. The relationship between plasma gradient scale length L_p and laser

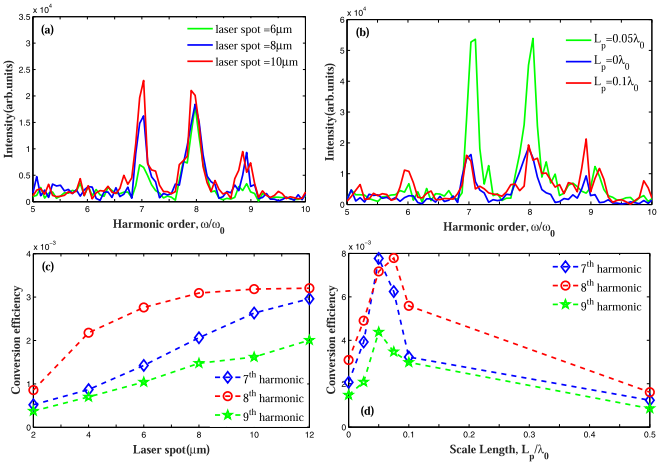

FIG. 7. The harmonic spectra generated at the emitting angle $\alpha = 17^\circ$ driven by the multicycle laser with different focal spot size (a) from the detuned plasma grating with different plasma gradient scale length L_p (b), the dependence of conversion efficiency of the harmonics on (c) the laser spot, and (d) plasma gradient scale length L_p. (a), (c) $\lambda_f = 100$ nm, $\beta = 15$ μm, $\tau = 20$ fs, $L_p = 0\lambda_0$; (b), (d) $\lambda_f = 100$ nm, $\beta = 15$ μm, $\tau = 20$ fs, laser spot is set to 8 μm.

prepulse has been experimentally and theoretically studied by Kahaly *et al.* [55]. The simulation results in Figs. 7(b) and 7(d) show the harmonic efficiency is the highest, when the scale length L_p is about $0.05\lambda_0$. In this work, the hypothesis of the simulations above by EPOCH does not include the ionization module. The influence of ionization module of EPOCH on harmonic intensity is presented in Figs. 8(a) and 8(b). The detuned grating target is made of carbon, the ionization energies are set to 11.26, 24.38, 47.89, 64.49, 392.1, and 490.0 eV. The results show the harmonic intensity simulated by EPOCH without the ionization module is higher than that with the ionization module. To consider the multidimensional effects, a 3D description of high harmonic generation is essential.

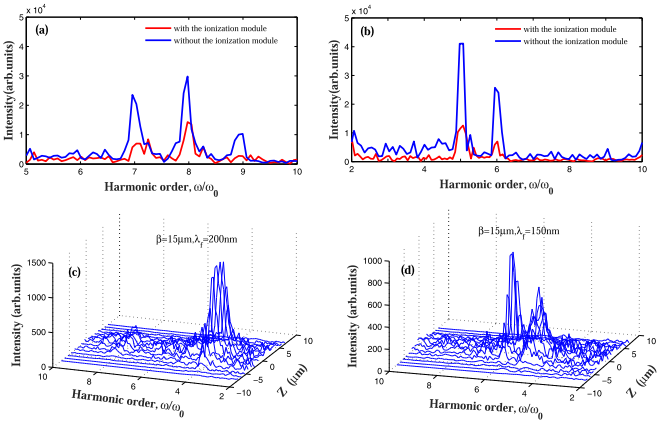

FIG. 8. The influence of ionization module of EPOCH on the harmonic intensity from detuned grating target with $\lambda_f = 100$ nm (a) and $\lambda_f = 150$ nm (b), the harmonics from detuned grating target with $\lambda_f = 200$ nm (c) and $\lambda_f = 150$ nm (d) simulated by 3D-EPOCH. (a), (b) $\beta = 15$ μm, $\tau = 20$ fs, the other parameters are the same as those in Fig. 5(c); (c), (d) $\beta = 15$ μm, $\tau = 20$ fs.

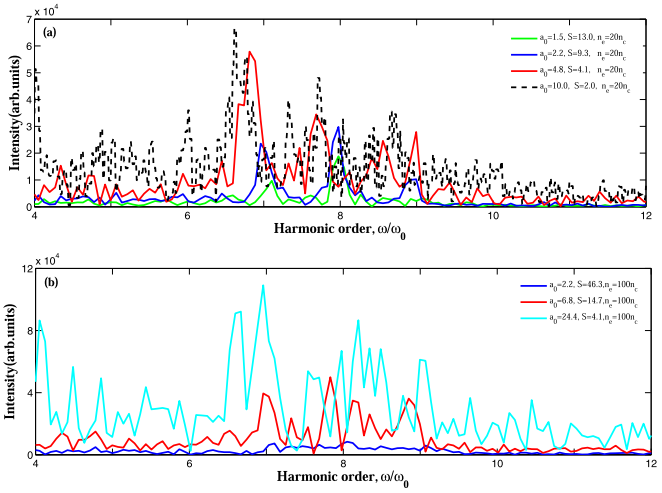

FIG. 9. The influence of laser intensity and electron density on the harmonic intensity from detuned grating target. (a) $a_0 = 1.5$, $a_0 = 2.2$, $a_0 = 4.8$, $a_0 = 10.0$ and n_e is set to $20n_c$. (b) $a_0 = 2.2$, $a_0 = 6.8$, $a_0 = 24.4$ and n_e is set to $100n_c$. $\lambda_f = 100$ nm, $\beta = 15$ μm, $\tau = 20$ fs, the other parameters are the same as those in Fig. 5(c).

Figures 8(c) and 8(d) show the harmonics from detuned grating target with different λ_f simulated by 3D-EPOCH; the size of the simulation box is $15\lambda_0 \times 15\lambda_0 \times 15\lambda_0$ corresponding to grids $3000(X) \times 500(Y) \times 500(Z)$, with eight macroparticles per cell, and the spatial resolution will limit the order number of the harmonics that can be observed below 10. The parameter β is set to 15 μm, λ_f is variational, the other parameters are the same as those in Fig. 5(c) simulated by 2D-PIC. Figures 8(c) and 8(d) show that a single-order harmonic with the order 4th is generated as λ_f is 200 nm, the harmonics with order from 5th to 6th are generated as λ_f is 150 nm. The results are in agreement with the results of Fig. 5(c). However, the intensity of the harmonic simulated by 3D-PIC is lower than the result simulated by 2D-PIC: this may be because of electron loss caused by the transverse forces of the laser pulse in the extra dimension [32,56].

Finally, the intensity of HHG from flat targets is relevant to the similarity parameter $S = n_e/(a_0 n_c)$, which was formulated by Gordienko *et al.* [57]. The conversion efficiency of harmonic emission from the grating target is considerably higher when the similarity parameter $S \simeq 4$ [45]. Figure 9(a) shows that the influence of laser intensity on the harmonic intensity from the detuned grating target with the electron density $n_e = 20n_c$, and the laser intensities are set to 5×10^{18}, 1×10^{19}, 5×10^{19}, and 2.14×10^{20} W/cm^2, respectively. It is seen that the red and black curves are higher than the other two curves, which means that the similarity parameter S with the lower values for the detuned grating target is optimum. When the electron density of the detuned grating target is set to near solid density, which is shown in Fig. 9(b), the results show that the harmonics is enhanced as the laser intensity is increased, while the harmonic spectrum becomes irregular and the noise is also enhanced.

The harmonics with particular frequencies in this work are generated to achieve compact XUV diffractive imaging [39], or as a narrow-band XUV source of x-ray excited inner-shell photoelectron (XPS) to study the electronic structure of condensed matter [40], or as a seed source for seeding a free-electron laser to produce fully coherent soft x rays [41]. From an experimental point of view, in order to generate narrow-band harmonics with specific frequencies, it is possible to use the detuned grating presented in this article with appropriate choices for λ_f and β. Such aperiodic structures can be fabricated by electron beam lithography or laser lithography [52]; however, the cost is very expensive.

IV. CONCLUSIONS

In conclusion, we have studied spectral characteristics of high-order harmonics by the interaction of a linearly polarized relativistic intensity laser pulse with a detuned plasma grating through particle-in-cell simulations and analytical model. The Fresnel zone plate with an aperiodic structure can only select low-order harmonics nearly parallel to the target surface. By introducing a correction factor β to the radius formula of the zone plate target, the match condition of harmonics at the narrow-band orders can be satisfied, and then only the narrow-band harmonics can appear nearly parallel to the target surface. The center frequency and linewidth of the narrow-band harmonics can be tuned by adjusting the parameters β and λ_f; the results show that adjusting the correction factor β is more beneficial to achieve spectrum control.

ACKNOWLEDGMENTS

This work was supported by the National Key R&D Program (Grant No. 2017YFA0206001), the National Natural Science Foundation of China (Grants No.12004353, No. 11975214, No. 11991071, No. 11905202, and No. 12174350), the National Key Research and Development Program of China (Grant No. 2017YFA0206004), anf Key Laboratory Foundation of The Sciences and Technology on Plasma Physics Laboratory (Grant No. 6142A04200103).

[1] P. M. Paul, E. S. Toma, P. Breger, G. Mullot, F. Augé, P. Balcou, H. G. Muller, and P. Agostini, Science **292**, 1689 (2001).

[2] M. Hentschel, R. Kienberger, C. Spielmann, G. A. Reider, N. Milosevic, T. Brabec, P. Corkum, U. Heinzmann, M. Drescher, and F. Krausz, Nature (London) **414**, 509 (2001).

[3] E. Goulielmakis, M. Uiberacker, R. Kienberger, A. Baltuska, V. Yakovlev, A. Scrinzi, Th. Westerwalbesloh, U. Kleineberg, U. Heinzmann, M. Drescher, and F. Krausz, Science **305**, 1267 (2004).

[4] B. Dromey, M. Zerf, A. Gopal, K. Lancaster, *et al.*, Nat. Phys. **2**, 456 (2006).

[5] Y. Nomura, R. Hörlein, P. Tzallas *et al.*, Nat. Phys. **5**, 124 (2009).
[6] J. A. Wheeler, A. Borot, S. Monchocé, H. Vincenti, A. Ricci, A. Malvache, R. Lopez-Martens, and F. Quéré, Nat. Photonics **6**, 829 (2012).
[7] B. Dromey, S. Rykovanov, M. Yeung *et al.*, Nat. Phys. **8**, 804 (2012).
[8] G. Ndabashimiye, S. Ghimire, M. Wu *et al.*, Nature (London) **534**, 520 (2016).
[9] A. Leblanc, S. Monchocé, S. Kahaly, F. Quéré, and C. Bourassin-Bouchet, Nat. Phys. **12**, 301 (2016).
[10] Y. Pertot, C. Schmidt, M. Matthews *et al.*, Science **355**, 264 (2017).
[11] A. R. Attar, A. Bhattacherjee, C. D. Pemmaraju *et al.*, Science **356**, 54 (2017).
[12] A. Moulet, J. B. Bertrand, T. Klostermann *et al.*, Science **357**, 1134 (2017).
[13] G. Sansone, E. Benedetti, F. Calegari *et al.*, Science **314**, 443 (2006).
[14] E. J. Takahashi, P. Lan *et al.*, Phys. Rev. Lett. **104**, 233901 (2010).
[15] P. Lan, P. Lu, Q. Li *et al.*, Phys. Rev. A **79**, 043413 (2009).
[16] P. B. Corkum, Phys. Rev. Lett. **71**, 1994 (1993).
[17] M. Lewenstein, P. Salieres, and A. LHuillier, Phys. Rev. A **52**, 4747 (1995).
[18] S. Y. Wang, W. Y. Hong *et al.*, Opt. Express **19**, 9986 (2011).
[19] C. Jin and C. D. Lin, Phys. Rev. A **85**, 033423 (2012).
[20] M. R. Edwards, V. T. Platonenko, and J. M. Mikhailova, Opt. Lett. **39**, 6823 (2014).
[21] G. Sansone, L. Poletto, and M. Nisoli, Nat. Photonics **5**, 655 (2011).
[22] M. Chini, K. Zhao, and Z. H. Chang, Nat. Photonics **10**, 1038 (2014).
[23] M. Yeung, S. Rykovanov, J. Bierbach *et al.*, Nat. Photonics **11**, 32 (2017).
[24] A. Leblanc, A. Denoeud, L. Chopineau, G. Mennerat, Ph. Martin, and F. Quéré, Nat. Phys. **13**, 440 (2017).
[25] A. Tarasevitch, K. Lobov *et al.*, Phys. Rev. Lett. **98**, 103902 (2007).
[26] B. Dromey, S. Kar, C. Bellei *et al.*, Phys. Rev. Lett. **99**, 085001 (2007).
[27] M. Bocoum, M. Thévenet, F. Böle, B. Beaurepaire, A. Vernier, G. Assanto, A. Jullien, J. Faure, and R. Lopez-Martens, Phys. Rev. Lett. **116**, 185001 (2016).
[28] F. Dollar, P. Cummings, V. Chvykov, L. Willingale, M. Vargas, V. Yanovsky, C. Zulick, A. Maksimchuk, A. G. R. Thomas, and K. Krushelnick, Phys. Rev. Lett. **110**, 175002 (2013).
[29] M. Behmke, D. an der Brügge, C. Rödel *et al.*, Phys. Rev. Lett. **106**, 185002 (2011).
[30] Y. X. Zhang, B. Qiao, X. R. Xu *et al.*, Phys. Plasmas **24**, 123119 (2017).
[31] Z. Y. Chen, Opt. Lett. **43**, 2114 (2018).
[32] Y. Zhang, B. Qiao, X. Xu *et al.*, Opt. Express **25**, 29058 (2017).
[33] S. Mirzanejadand M. Salehi, Phys. Rev. A **87**, 063815 (2013).
[34] G. Ma, W. Dallari, A. Borot *et al.*, Phys. Plasmas **22**, 033105 (2015).
[35] F. Quéré, C. Thaury, P. Monot, S. Dobosz, and P. Martin, J. P. Geindre, and P. Audebert, Phys. Rev. Lett. **96**, 125004 (2006).
[36] H. Vincenti and F. Quéré, Phys. Rev. Lett. **108**, 113904 (2012).
[37] C. M. Heyl, S. N. Bengtsson, S. Carlström, J. Mauritsson, C. L. Arnold, and A. L'Huillier, New J. Phys. **16**, 052001 (2014).
[38] O. Jahn, V. E. Leshchenko, P. Tzallas *et al.*, Optica **6**, 280 (2019).
[39] R. L. Sandberg, A. Paul, D. A. Raymondson, S. Hädrich, D. M. Gaudiosi, J. Holtsnider, R. I. Tobey, O. Cohen, M. M. Murnane, H. C. Kapteyn, C. Song, J. Miao, Y. Liu, and F. Salmassi, Phys. Rev. Lett. **99**, 098103 (2007).
[40] A. Romanyuk, R. Steiner, L. Marot, and P. Oelhafen, Sol. Energy Mater. Sol. Cells **91**, 1831 (2007).
[41] E. Allaria, R. Appio, L. Badano, W. A. Barletta, S. Bassanese, S. G. Biedron, A. Borga, E. Busetto, D. Castronovo, P. Cinquegrana, S. Cleva *et al.*, Nat. Photonics **6**, 699 (2012).
[42] Z. Y. Chen, Phys. Rev. E **97**, 043202 (2018).
[43] B. Dromey, S. G. Rykovanov, D. Adams, R. Hörlein, Y. Nomura, D. C. Carroll, P. S. Foster, S. Kar, K. Markey, P. McKenna, D. Neely, M. Geissler, G. D. Tsakiris, and M. Zepf, Phys. Rev. Lett. **102**, 225002 (2009).
[44] X. Lavocat-Dubuis and J. -P. Matte, Phys. Rev. E **80**, 055401(R) (2009).
[45] X. Lavocat-Dubuis and J. -P. Matte, Phys. Plasmas **17**, 093105 (2010).
[46] M. Cerchez, A. L. Giesecke, C. Peth *et al.*, Phys. Rev. Lett. **110**, 065003 (2013).
[47] G. Cantono, L. Fedeli, A. Sgattoni, A. Denoeud, L. Chopineau, F. Rëau, T. Ceccotti, and A. Macchi, Phys. Rev. Lett. **120**, 264803 (2018).
[48] M. Yeung, B. Dromey, C. Rödel *et al.*, New J. Phys. **15**, 025042 (2013).
[49] L. Fedeli, A. Sgattoni, G. Cantono *et al.*, Appl. Phys. Lett. **110**, 051103 (2017).
[50] Y. Wang, H. Song, H. Liu *et al.*, Phys. Plasmas **24**, 083107 (2017).
[51] S. J. Zhang, H. B. Zhuo, D. B. Zou *et al.*, Phys. Rev. E **93**, 053206 (2016).
[52] H. Li, L. Shi, L. Wei, C. Xie, and L. Cao, Appl. Phys. Lett. **110**, 041104 (2017).
[53] S. Monchocé, S. Kahaly, A. Leblanc, L. Videau, P. Combis, F. Réau, D. Garzella, P. D'Oliveira, Ph. Martin, and F. Quéré, Phys. Rev. Lett. **112**, 145008 (2014).
[54] T. D. Arber, K. Bennett, C. S. Brady *et al.*, Plasma Phys. Controlled Fusion **57**, 113001 (2015).
[55] S. Kahaly, S. Monchocé, H. Vincenti, T. Dzelzainis, B. Dromey, M. Zepf, Ph. Martin, and F. Quéré, Phys. Rev. Lett. **110**, 175001 (2013).
[56] M. Geissler, S. Rykovanov, J. Schreiber, J. Meyer-ter-Vehn, and G. D. Tsakiris, New J. Phys. **9**, 218 (2007).
[57] S. Gordienko and A. Pukhov, Phys. Plasmas **12**, 043109 (2005).